Supporting Information for Analytical Chemistry

Microfluidic pipette tip for high-purity and high-throughput blood plasma separation from whole blood

Byeongyeon Kim, Sein Oh, Dongwon You, and Sungyoung Choi

1. Supporting Experimental Method

Fabrication and principle of the smart pipette. The smart pipette was fabricated by assembling a conventional 1-mL pipette tip as a liquid-holding chamber, a 3D-printed air chamber, and a 60 mL BD syringe (Figure S4). The air chamber and a plunger holder were printed using a Mojo 3D printer (Stratasys, USA). After acetone treatment, the chamber was coated with a thin layer of epoxy to prevent air leakage. A 3D printing technology based on fused deposition modeling (FDM) was used for production of the air-chamber part of the smart pipette due to the availability. In principle, the fabrication method can generate fine pores between deposed layers so that the downstream processing such as acetone treatment is required for sealing the pores and creating the airtight smart pipette.[S1] The downstream processing can be omitted by using a stereolithography (SLA)-based 3D printer which can generate smooth, seamless structures.[S1] For smart-pipetting to separate blood plasma, 1.5 mL of whole blood was first drawn into the 1-mL pipette tip of the smart pipette by pulling the plunger (Figure S5). At this time, the plunger was set to a certain graduation of the syringe (V_1 = 40 mL). The microfluidic pipette tip was then assembled onto the end of the 1 mL-pipette tip. Fully depressing the plunger and locking its position with the plunger holder generated an average flow rate of 904.3 ± 15.6 μL min^{-1}. The air chamber of 12 mL in the inner volume (V_2) acts as a pressure buffer, maintaining a set pressure or a set flow rate within a narrow range. As soon as the plunger is fully depressed, a positive pressure (P) can be generated and defined as

$$P = \frac{V_1}{V_2} P_{atm} \quad (1)$$

, where P_{atm} is the atmospheric pressure. The pressure gradually decreases as blood exits though the microfluidic pipette tip and thus the air volume, V_2 expands to $V_2 + \Delta V_3$, and the changing pressure (P_c) can be defined as

$$P_c = \frac{V_1}{V_2 + \Delta V_3} P_{atm} \quad (2)$$

At V_2 = 12 mL and $(\Delta V_3)_{max}$ = 1 mL, the smart pipette can theoretically maintain the difference between P and P_c of below 8%.

Computational fluid dynamic simulation. 3D finite element models were built over the same dimensions as the CSA and DSA devices and then solved using Comsol Multiphysics (Comsol, USA) (Figure S2). No-slip boundary conditions were applied at the device walls, the constant flow rate of 100 µL min^{-1} was applied at the inlet, and the pressure at the outlet was fixed at atmospheric pressure. In the finite element models, the Navier-Stokes equation was solved and the simulation results were post-processed to visualize velocity vectors.

2. Supporting Text

Performance comparison of plasma separation methods. Centrifugation is the standard method for preparing blood plasma by packing blood cells under centrifugal force and collecting the resulting supernatant. The conventional method requires a bench-top centrifuge which typically prevents point-of-care tests and increases the cost of sample preparation. To address the above challenge, centrifugation-based plasma separators have been developed by utilizing a hand-powered egg beater[S2] and a compact-disk platform.[S3] These methods can obviate the need for costly equipment, thereby enabling cost-effective sample preparation and facilitating their use in point-of-care settings. Filtration methods have been also employed for cost-effective and equipment-free separation of blood plasma from whole blood.[S4-S6] Both centrifugation-based and filtration approaches enable blood plasma separation with high purity and collection efficiency. However, these methods may not be suitable for large-scale sample preparation due to the limited separation capacity and discontinuous separation processes. Although continuous-flow plasma separators have the potential for rapid and large-scale plasma preparation,[S7-S9] they tend to suffer from low plasma collection efficiency due to the inability to densely pack blood cells in a continuous flow. The proposed platform also exhibits a relatively low plasma recovery, as compared with plasma separators based on centrifugation and filtration. Further improvement in plasma recovery can be achieved by repeating the separation

process with the sorted blood in the RBC reservoir. The throughput capability of the proposed platform is considerably higher than other state of the art microfluidic separators, while maintaining high plasma quality. Since the separation channels of the microfluidic pipette tip are readily scalable, further throughput enhancement can be easily achieved by massive parallelization for large-scale blood processing.

3. Supporting Table

Table S1. Summary of continuous-flow, whole-blood plasma separators.

Principles	Purity (%)	Throughput (μL min^{-1})	Plasma extraction rate (μL min^{-1})
Acoustic separation [11]	≈100	80	10
Microfiltration [13]	≈100	>0.83	-
Deterministic lateral displacement [14]	≈100	≈0.4	-
Inertial microfluidics [15]	99.5	500	5-30
Zweifach-Fung [16]	99	33.3	≈1.67
Hydrophoresis [17]	93	100.9	12.1
This work	99.88	904.3	51

4. Supporting Figures

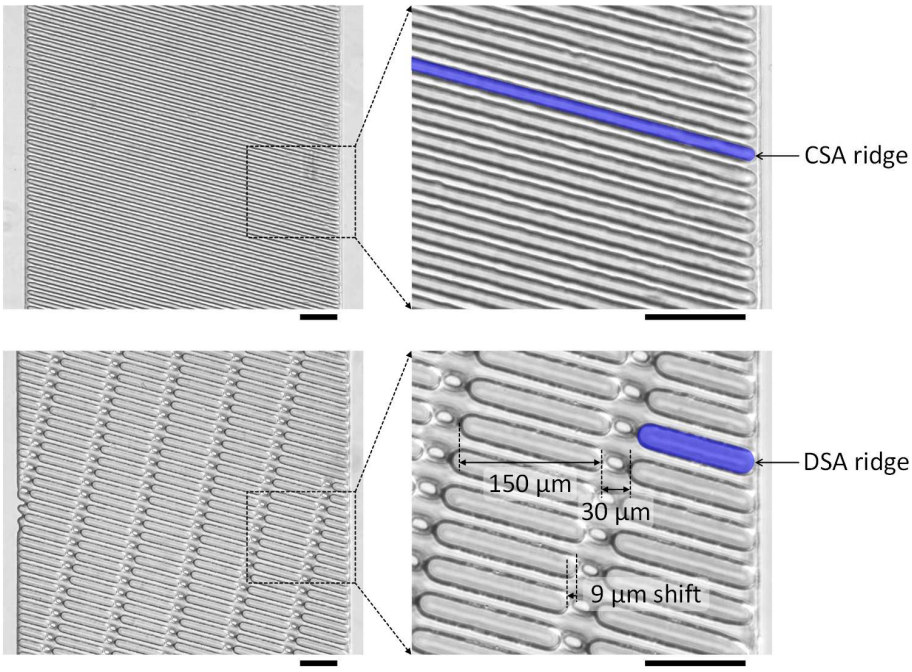

FIG. S1. Micrographs showing (top) continuous slant array ridges and (bottom) discrete slant array ridges with specified dimensions (scale bars, 100 µm).

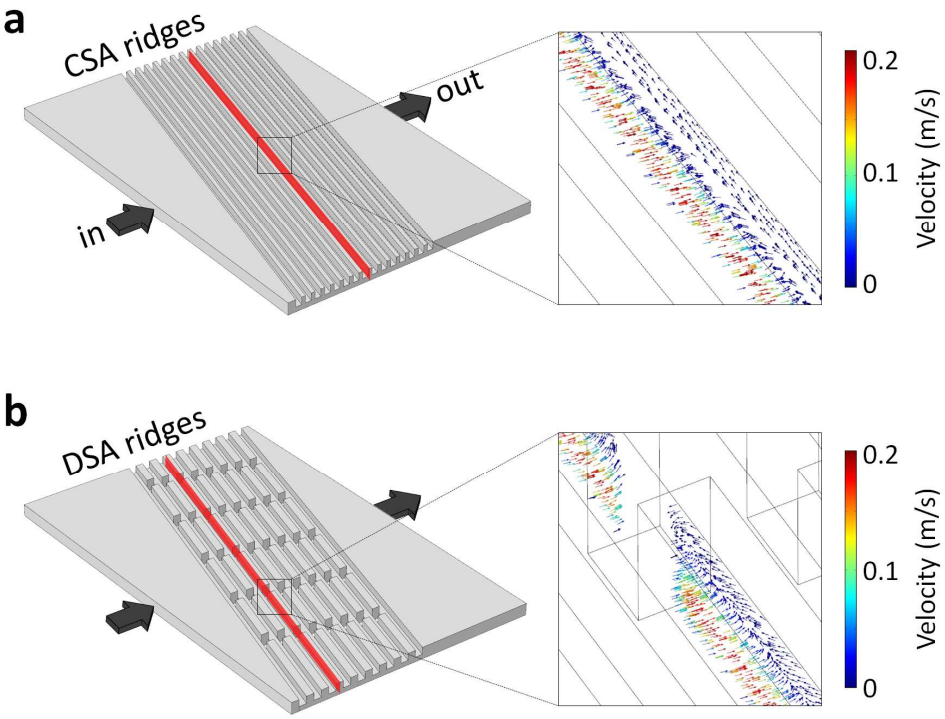

FIG. S2. Flow simulations. (a, b) Simulated velocity vectors on the cross-sections in (a) the CSA device and (b) the DSA device.

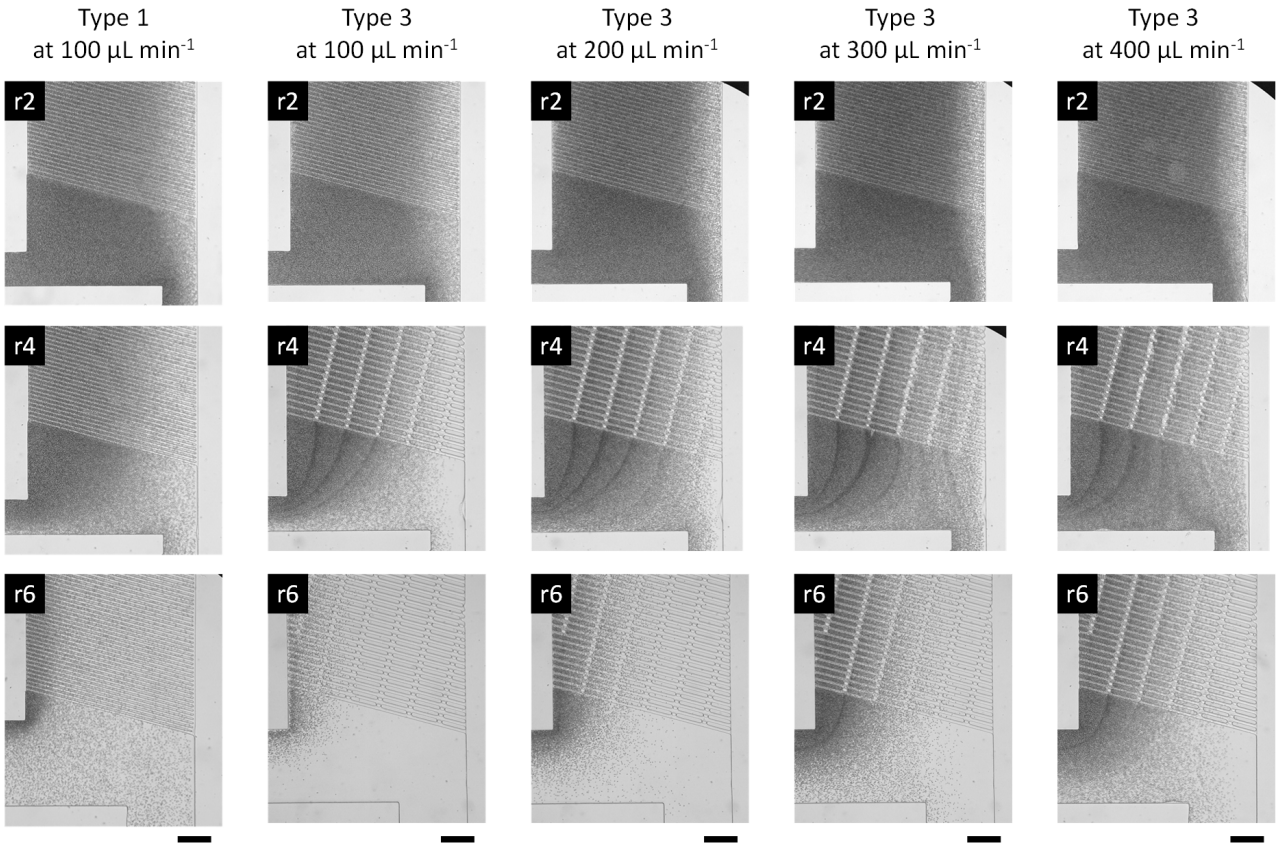

FIG. S3. Micrographs showing RBC focusing behaviors in the type 1 and type 3 devices. In the type 3 device, plasma separation from whole blood is affected by flow rate. The flow direction is from top to bottom in each image. Scale bars, 200 µm.

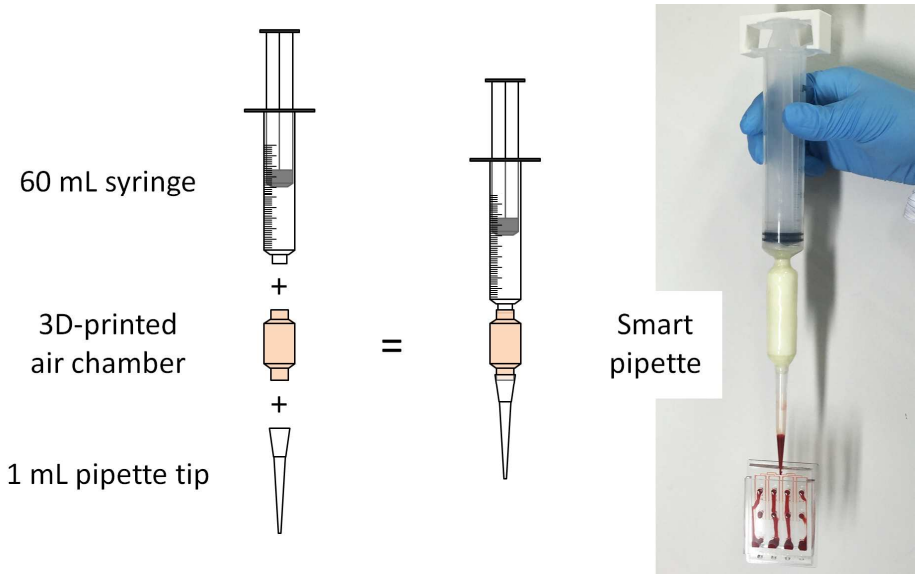

FIG. S4. The smart pipette was fabricated by assembling the three major parts: a liquid-holding tip (1-mL pipette tip), a 3D-printed air chamber and a 60-mL syringe.

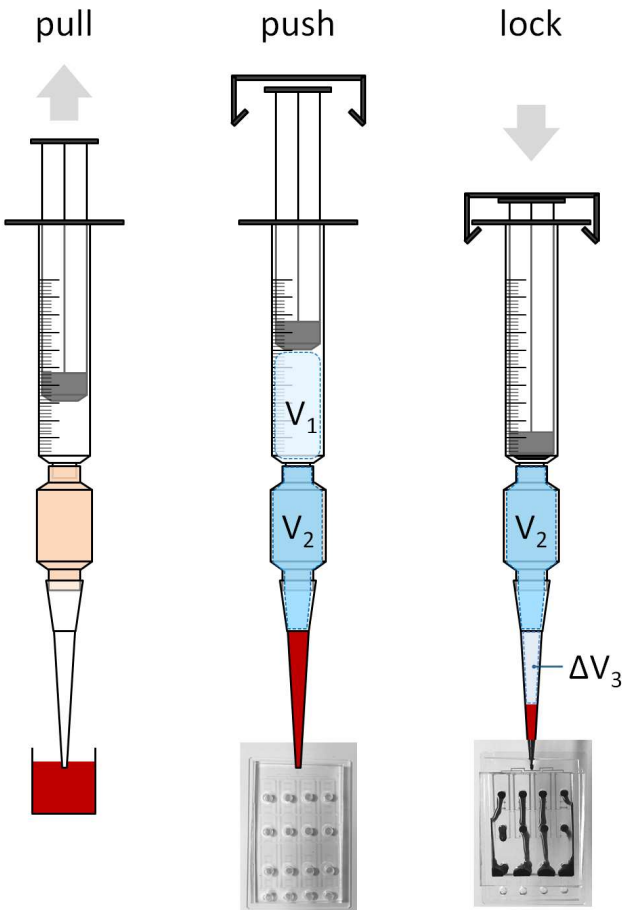

FIG. S5. Smart pipetting procedures for blood plasma separation. After blood is drawn into the liquid-holding tip, the microfluidic pipette tip for blood plasma separation is attached to the smart pipette. Pushing the plunger generates a pressure-driven flow through the microfluidic pipette tip and enables high-purity and high-throughput plasma separation.

5. Supporting References

(S1) Au, A. K.; Huynh, W.; Horowitz, L. F.; Folch, A. *Angew. Chem., Int. Ed.* **2016**, *55*, 3862-3881.

(S2) Wong, A. P.; Gupta, M.; Shevkoplyas, S. S.; Whitesides, G. M. *Lab Chip* **2008**, *8*, 2032-2037.

(S3) Haeberle, S.; Brenner, T.; Zengerle, R.; Ducree, J. *Lab Chip* **2006**, *6*, 776-781.

(S4) Gong, M. M.; MacDonald, B. D.; Nguyen, T. V.; Van Nguyen, K.; Sinton, D. *Biomicrofluidics* **2013**, *7*, 044111.

(S5) Liu, C.; Liao, S. C.; Song, J.; Mauk, M. G.; Li, X.; Wu, G.; Ge, D.; Greenberg, R. M.; Yang, S.; Bau, H. H. *Lab Chip* **2016**, *16*, 553-560.

(S6) Liu, C.; Mauk, M.; Gross, R.; Bushman, F. D.; Edelstein, P. H.; Collman, R. G.; Bau, H. H. *Anal. Chem.* **2013**, *85*, 10463-10470.

(S7) Lenshof, A.; Ahmad-Tajudin, A.; Järås, K.; Swärd-Nilsson, A. M.; Åberg, L.; Marko-Varga, G.; Malm, J.; Lilja, H.; Laurell, T. *Anal. Chem.* **2009**, *81*, 6030-6037.

(S8) Tripathi, S.; Kumar, Y. V.; Agrawal, A.; Prabhakar, A.; Joshi, S. S. *Sci. Rep.* **2016**, *6*, 26749.

(S9) Kim, B.; Choi, S. *Small* **2016**, *12*, 190-197.